NASA/CR—2010-216748

Microstructure Modeling of Third Generation Disk Alloys

Final Report

Herng-Jeng Jou
QuesTek Innovations LLC, Evanston, Illinois

July 2010

NASA STI Program . . . in Profile

Since its founding, NASA has been dedicated to the advancement of aeronautics and space science. The NASA Scientific and Technical Information (STI) program plays a key part in helping NASA maintain this important role.

The NASA STI Program operates under the auspices of the Agency Chief Information Officer. It collects, organizes, provides for archiving, and disseminates NASA's STI. The NASA STI program provides access to the NASA Aeronautics and Space Database and its public interface, the NASA Technical Reports Server, thus providing one of the largest collections of aeronautical and space science STI in the world. Results are published in both non-NASA channels and by NASA in the NASA STI Report Series, which includes the following report types:

- TECHNICAL PUBLICATION. Reports of completed research or a major significant phase of research that present the results of NASA programs and include extensive data or theoretical analysis. Includes compilations of significant scientific and technical data and information deemed to be of continuing reference value. NASA counterpart of peer-reviewed formal professional papers but has less stringent limitations on manuscript length and extent of graphic presentations.

- TECHNICAL MEMORANDUM. Scientific and technical findings that are preliminary or of specialized interest, e.g., quick release reports, working papers, and bibliographies that contain minimal annotation. Does not contain extensive analysis.

- CONTRACTOR REPORT. Scientific and technical findings by NASA-sponsored contractors and grantees.

- CONFERENCE PUBLICATION. Collected papers from scientific and technical conferences, symposia, seminars, or other meetings sponsored or cosponsored by NASA.

- SPECIAL PUBLICATION. Scientific, technical, or historical information from NASA programs, projects, and missions, often concerned with subjects having substantial public interest.

- TECHNICAL TRANSLATION. English-language translations of foreign scientific and technical material pertinent to NASA's mission.

Specialized services also include creating custom thesauri, building customized databases, organizing and publishing research results.

For more information about the NASA STI program, see the following:

- Access the NASA STI program home page at *http://www.sti.nasa.gov*

- E-mail your question via the Internet to *help@sti.nasa.gov*

- Fax your question to the NASA STI Help Desk at 443–757–5803

- Telephone the NASA STI Help Desk at 443–757–5802

- Write to:
  NASA Center for AeroSpace Information (CASI)
  7115 Standard Drive
  Hanover, MD 21076–1320

NASA/CR—2010-216748

Microstructure Modeling of Third Generation Disk Alloys

Final Report

Herng-Jeng Jou
QuesTek Innovations LLC, Evanston, Illinois

Prepared under Contract NNC07CB01C

National Aeronautics and
Space Administration

Glenn Research Center
Cleveland, Ohio 44135

July 2010

Level of Review: This material has been technically reviewed by NASA technical management.

Available from

NASA Center for Aerospace Information
7115 Standard Drive
Hanover, MD 21076–1320

National Technical Information Service
5301 Shawnee Road
Alexandria, VA 22312

Available electronically at http://gltrs.grc.nasa.gov

Microstructure Modeling of Third Generation Disk Alloys
Final Report

Herng-Jeng Jou
QuesTek Innovations LLC
Evanston, Illinois 60201

Executive Summary

The objective of this program was to model, validate, and predict the precipitation microstructure evolution, using *PrecipiCalc* (QuesTek Innovations LLC) software, for 3rd generation Ni-based gas turbine disc superalloys during processing and service, with a set of logical and consistent experiments and characterizations. Furthermore, within this program, the originally research-oriented microstructure simulation tool was to be further improved and implemented to be a useful and user-friendly engineering tool.

In this report, the key accomplishments achieved during the third year (2009) of the program are summarized. The activities of this year included:

- Further development of multistep precipitation simulation framework for γ' microstructure evolution during heat treatment
- Calibration and validation of γ' microstructure modeling with supersolvus heat treated LSHR
- Modeling of the microstructure evolution of the minor phases, particularly carbides, during isothermal aging, representing the long term microstructure stability during thermal exposure
- The implementation of software tools.

During the research and development efforts to extend the precipitation microstructure modeling and prediction capability in this 3-year program, we identified a hurdle, related to slow γ′ coarsening rate, with no satisfactory scientific explanation currently available. It is desirable to raise this issue to the Ni-based superalloys research community, with hope that in future there will be a mechanistic understanding and physics-based treatment to overcome the hurdle. In the mean time, an empirical correction factor was developed in this modeling effort to capture the experimental observations.

The established modeling capability and software tools at the end of this program represent state-of-the-art precipitation modeling and simulation for Ni-based aeroturbine disk superalloys under complex industrial heat treatment. While model calibration/validation was mainly established with data of NASA's LSHR alloy, the resulting models and tools provide a solid foundation to model other disk alloys. Currently, further application to Rolls-Royce's RR1000 alloy is underway. We expect these models and tools, through use and testing by materials engineers, to be further improved in the future. By utilizing these tools, novel process and microstructure optimization can be virtually and effectively developed for the 3rd generation gas turbine disc alloys to enable accelerated material development.

Contents

Introduction

Predictive science-based computational materials modeling and tools have great potential to accelerate process optimization of 3rd generation Ni-base superalloys in gas turbine disk applications. By extending the DARPA-AIM methodology, previously demonstrated in disc alloys IN100 and R88DT (Refs. 1 and 2), this NASA Aviation Safety Program aimed to establish logical calibration, validation and user-friendly implementation of *PrecipiCalc*, a multicomponent multiphase precipitation simulation software, for four 3rd generation nickel-based disk superalloys: ME3 (also called René104), LSHR (Low-Solvus, High-Refractory alloy developed by NASA), Alloy 10 (developed by Honeywell), and RR1000 (developed by Rolls-Royce). The nominal compositions for these alloys are listed in Table 1.

TABLE 1.—NOMINAL COMPOSITIONS OF THE FOUR THIRD GENERATION DISC ALLOYS, IN wt%, STUDIED UNDER THIS PROGRAM

wt%	Ni	Cr	Co	Mo	W	Al	Ti	Nb	Ta	Hf	C	B	Zr
ME3	Bal.	13.1	20.0	3.8	1.9	3.5	3.6	1.1	2.3	–	0.040	0.030	0.05
LSHR	Bal.	13.0	21.0	2.7	4.3	3.5	3.5	1.5	1.6	–	0.030	0.030	0.05
Alloy10	Bal.	10.2	14.9	2.7	6.2	3.7	3.9	1.9	0.9	–	0.030	0.030	0.10
RR1000	Bal.	15.0	18.5	5.0	–	3.0	3.6	–	2.0	0.5	0.027	0.015	0.06

The program was completed at the end of 2009, and this report summarizes the key results in the third year (2009) of this program. The major activities conducted in 2009 are shown in the Gantt chart (see Figure 1). The project team includes NASA Glenn Research Center (GRC), QuesTek, AFRL (as scientific advisor), Rolls-Royce (as industrial advisor), and University of Cambridge. Regular monthly teleconferences among the project team and monthly reports were facilitated to enhance communication.

The main activities in 2009 are Tasks 2 to 5, and the subsequent sections of this report summarize the activities and results. Due to a change in the priority focus of this program, the resource originally planned for Task 6—"Microstructure Variation and Optimization" was shifted to other higher priority Tasks, particular Tasks 4 and 5.

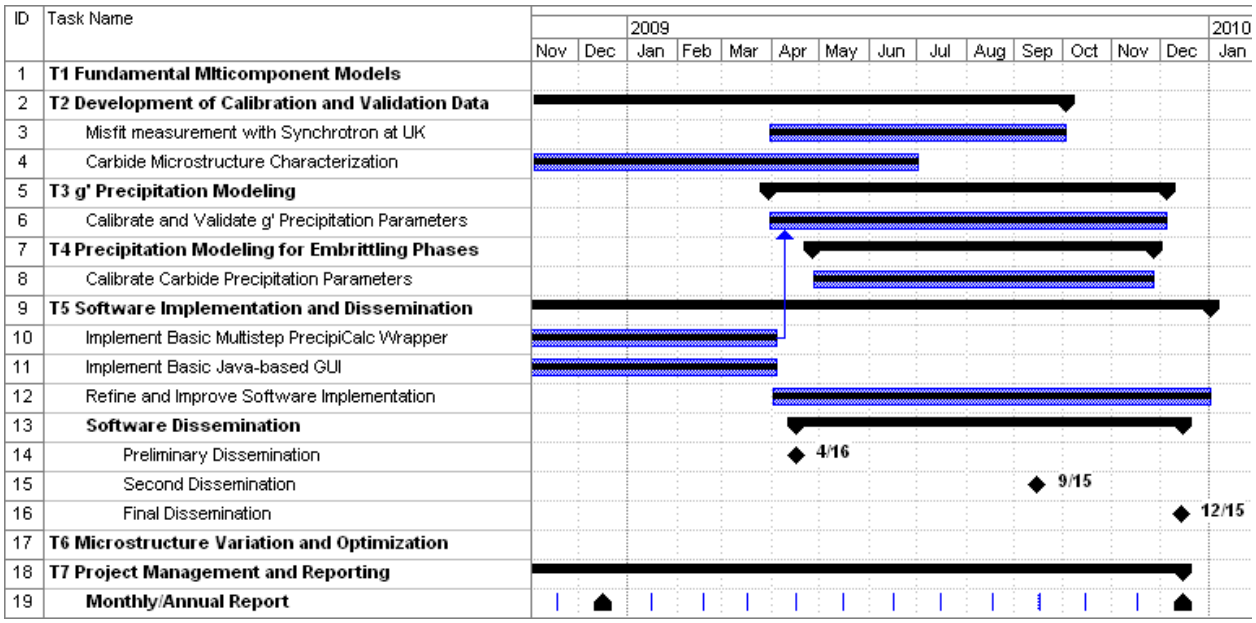

Figure 1.—Gantt chart of the third year of this program.

Task 2—Development of Calibration and Validation Data

The focus of Task 2 was to develop necessary experimental data for the calibration and validation of models established in Task 3 and 4. Two previous annual reports (Refs. 3 and 4) summarize the data development in the first two years (2007 and 2008) of this program. In 2009, the experimental study focused on the following two areas.

- γ/γ' Misfit Measurement—in addition to the misfit measurement by x-ray diffraction conducted at GRC (summarized in Ref. 4), University of Cambridge has conducted synchrotron and neutron diffraction characterization of both LSHR and Alloy10 samples. The LSHR data will be discussed in the Task 3 effort.
- Carbide Microstructure Characterization—carbides, and other minor phases, in LSHR samples were studied by GRC under different aging conditions. The results will be discussed in detail in Task 4.

Task 3—γ' Precipitation Modeling

Ni-based aeroturbine disk superalloys rely on a multiscale γ' precipitate microstructure to achieve a suitable combination of mechanical properties. As heat treatment has a substantial impact on the γ' microstructure, the capability of simulating γ' size and fraction evolution is strongly desirable for disk alloy development. Continuing the efforts in the first two years of this program, the focus of the last year was the development and calibration/validation of the multistep *PrecipiCalc* framework.

Interaction of Secondary and Tertiary γ' in Isothermal Aging

The mean field approximation and theory used in *PrecipiCalc* models for computational efficiency have limitations, which have been identified in the DARPA AIM initiative (Ref. 5) in addition to this program. Under the mean field assumption, every particle interacts with all other particles instantaneously through common mean matrix compositions. This assumption is reasonable for single modal randomly-arranged precipitate distribution under nucleation, growth, or coarsening. For a multimodal distribution, such as γ' precipitates in Ni-based aeroturbine disk superalloys, number density variation and spatial arrangement limits the diffusional interaction and the particle coarsening kinetics deviate from that predicted by the mean field theory. This subsection describes a semi-empirical modeling approach to correct the results obtained from predictions using the mean field approximation.

With a multimodal distribution, a single large particle (low number density) is typically surrounded by many small particles (high number density), see Figure 2(a) for a schematic illustration with one secondary particle surrounded by many tertiary γ' particles. The aforementioned approach also applies to the primary and the secondary γ' particles. The large secondary γ' particle can only interact diffusionally with the tertiary particles within a region represented by a spherical radius, R_S, which is larger than the radius representing precipitate free zone, R_{PFZ}. Due to the interaction with large secondary γ', the tertiary γ' within the shell region ($R_{PFZ} < R < R_S$) are dissolving to feed the growth of the larger particle. But the growth rate of secondary particle is lower than that predicted by mean field theory, see Figure 2(b) for a schematic illustration. Tertiary γ' particles away from the shell region, on the other hand, do not experience the field of large secondary particle, and coarsen as if there are only tertiary particles.

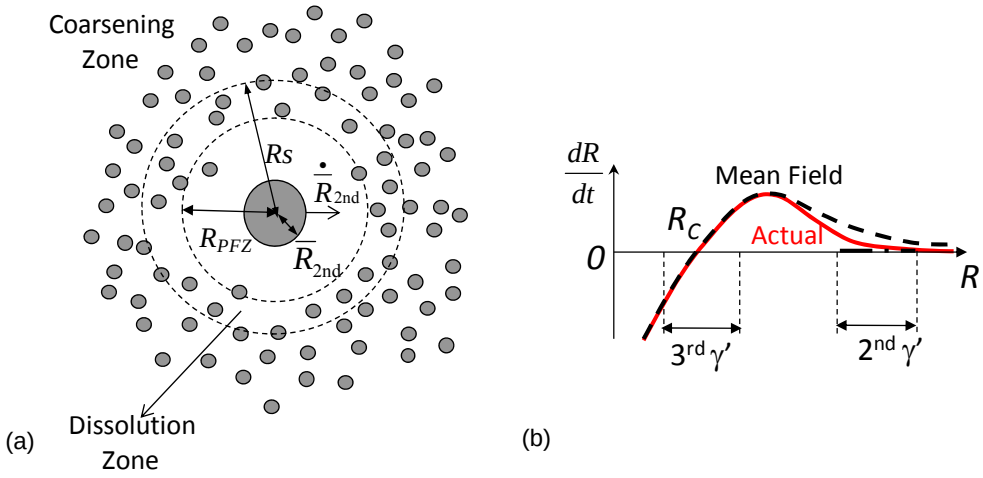

Figure 2.—Schematic diagrams of (a) a large secondary γ' particle surrounded by many tertiary γ' particles, and (b) particle growth rate versus particle radii comparing mean field prediction and actual growth rates under coarsening.

Under the DARPA AIM initiative (Ref. 5), an approach involving multistep *PrecipiCalc* and freezing large γ' particles was utilized to overcome the mean field limitation, which had caused overgrowth of the large γ' particles during cooling and coarsening. This approach involves a series of multiple *PrecipiCalc* calculations, removal of large γ' particles, and subsequent coarsening simulations considering only smaller γ' particles. By freezing out the large particles and prohibiting communication between the two populations of particles, the growth potency of the large γ' particles are suppressed during isothermal aging. However, GRC's experimental evidence did indicate that ignoring the growth of large γ' particles is not a good assumption. In this program, we have further refined and extended the approach developed under AIM to account for the communication of multimodal distributions under coarsening.

The new approach to incorporate the interaction between secondary and tertiary γ' particles during isothermal aging was formulated by post-processing the results obtained by considering only tertiary γ' coarsening (with secondary γ' removed from the calculation). Based on the mean size ($\bar{R}$) and mean field growth rate ($\dot{\bar{R}}_{2nd,MeanField}$) at the beginning of coarsening (denoted *t=0*), the actual growth rate, $\dot{\bar{R}}_{2nd}$, of supercritical secondary γ' was semi-empirically derived in the following equations:

$$R_{PFZ} = C_1 \bar{R}_{2nd}$$

$$R_S = C_2 \bar{R}_{2nd}$$

$$\dot{\bar{R}}_{2nd,MeanField}(t) = \dot{\bar{R}}_{2nd,MeanField}(t=0)\frac{\bar{R}_{2nd}(t=0)}{\bar{R}_{2nd}(t)}$$

$$\begin{aligned}\dot{\bar{R}}_{2nd} &\sim \dot{\bar{R}}_{2nd,MeanField}(t)\frac{1}{(R_{PFZ})^2}\frac{N_{3rd\ and\ inside\ R_S}}{N_{3rd}(t=0)} \\ &\sim \left[\dot{\bar{R}}_{2nd,MeanField}(t=0)\frac{\bar{R}_{2nd}(t=0)}{\bar{R}_{2nd}(t)}\right]\left[\frac{1}{(R_{PFZ})^2}\right]\left[\frac{4\pi}{3}\left(R_s^3 - R_{PFZ}^3\right)\right] \qquad (1) \\ \dot{\bar{R}}_{2nd} &= \text{Constant} \times \left[\dot{\bar{R}}_{2nd,MeanField}(t=0) \times \bar{R}_{2nd}(t=0)\right]\end{aligned}$$

This allowed us to reduce the correction down to a single fitting parameter. With calculations for the growth rate of secondary γ', the corresponding changes to the volume fractions of secondary and tertiary γ' could be determined through geometric corrections:

$$\overline{R}_{2\mathrm{nd}}(t) = \overline{R}_{2\mathrm{nd}}(t=0) + \dot{\overline{R}}_{2\mathrm{nd}} \times t$$

$$f_{2\mathrm{nd}}(t) = \frac{4\pi}{3}\left(\overline{R}_{2\mathrm{nd}}(t)\right)^3 N_{2\mathrm{nd}}$$

$$f_{3\mathrm{rd}}(t) = \left[f_{2\mathrm{nd}}(t=0) + f_{3\mathrm{rd}}(t=0)\right] - f_{2\mathrm{nd}}(t)$$

Note that the mean size of the tertiary particles was already determined by the coarsening simulation of the tertiary particles alone.

Multistep *PrecipiCalc* Simulation Framework for γ' Precipitation

To enable the freezing and post-processing correction discussed in the previous subsection, a sequential multistep *PrecipiCalc* simulation framework was required. Simulation structure for a thermo-mechanical and heat treatment cycle with two aging steps required a total of six sequential *PrecipiCalc* simulations, as shown in Figure 3. During the two isothermal aging steps (nos. 3 and 5), the communication between secondary and tertiary γ' (or primary and secondary γ') was captured using the framework discussed in the previous section. This sequential operation involved tedious mass balance and careful setup of *PrecipiCalc* calculations. Hence, it has been automated in a software wrapping program, which will be discussed in Task 5.

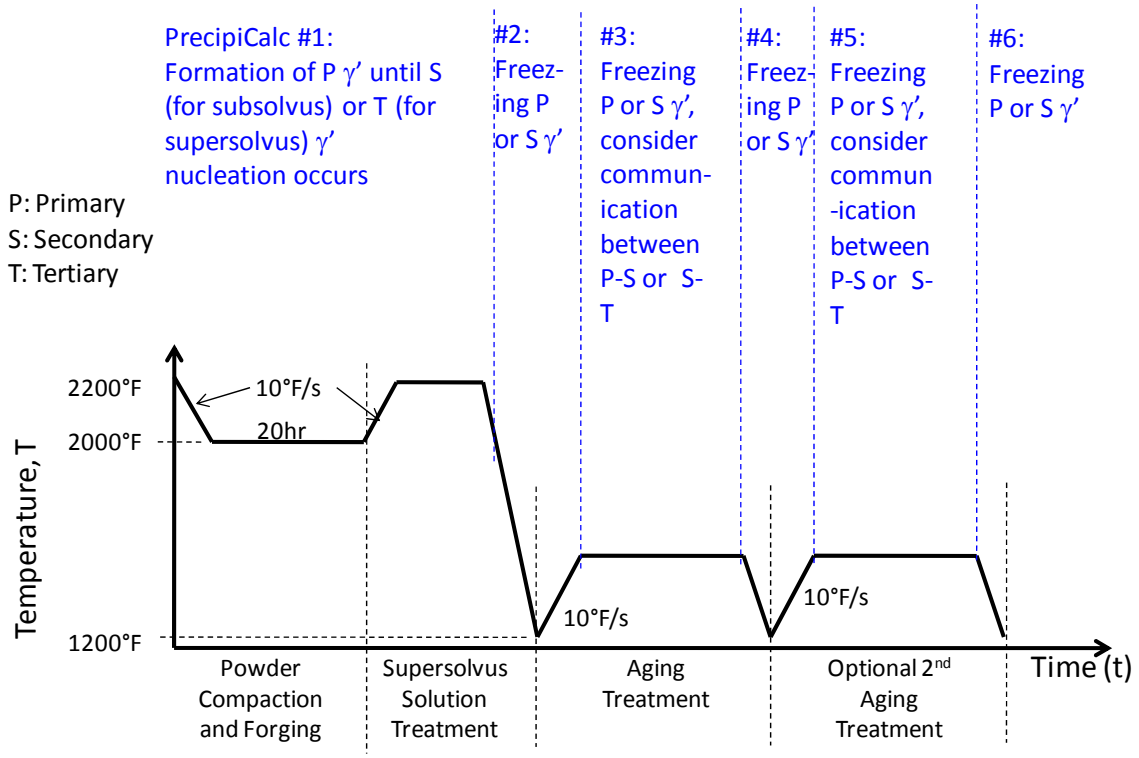

Figure 3.—Schematic multistep *PrecipiCalc* simulation framework with respect to the heat treatment history.

Calibration and Validation of γ' Microstructure Modeling for Supersolvus LSHR

A portion of the microstructure characterization results published in the NASA study of supersolvus LSHR (Ref. 6) was selected, see Table 2, to calibrate the multistep *PrecipiCalc* framework established earlier. The setup of the multistep *PrecipiCalc* simulation is summarized below.

- LSHR lookup table data was generated based on Ni-3.4Al-12.9Cr-21.3Co-3.67Ti-2.66Mo-4.3W-1.35Nb-1.66Ta-0.048Zr-0.024C-0.03B (in wt%) with carbides and borides eliminated;
- Two controlled cooling rates after the supersolvus treatment were 202 °C/min (3.67 °C/s) and 72 °C/min (1.2 °C/s), according to the NASA study (Ref. 6). Only the fast cooling (202 °C/min) data (as in Table 2) were used for calibration purposes;
- The cooling rate after the aging was assumed to be 11 °C/min (0.183 °C/s) for all samples;
- The heating rate to solution treatment or aging was assumed to be 10 °F/s (5.56 °C/s) for all samples;
- All non-isothermal heating and cooling were assumed to be linear for all samples, though in reality the cooling were more likely Newtonian; and
- Simulations started from the heatup to the solution treatment (without forging/extrusion portion illustrated in Figure 3) and no γ' particles were assumed to exist at the start of the simulations. This is a valid assumption as the subsequent 1171 °C/4 hr supersolvus treatment eliminates primary γ' particles anyway.

TABLE 2.—SELECTED γ' MICROSTRUCTURE FROM SUPERSOLVUS TREATED LSHR (REF. 6) USED FOR MODEL CALIBRATION

Solution treat	Age 1	Age 2
1171 °C + 202 °C/m	0	0
1171 °C + 202 °C/m	815 °C/3 hr	0
1171 °C + 202 °C/m	815 °C/8 hr	0
1171 °C + 202 °C/m	855 °C/1 hr	775 °C/8 hr
1171 °C + 202 °C/m	855 °C/4 hr	775 °C/8 hr
1171 °C + 202 °C/m	855 °C/8 hr	775 °C/8 hr

The calibration facilitated the determination of the following three main parameters:

- Surface energy was determined to be 0.025 J/m^2 which is within the range 0.0225 to 0.0315 J/m^2 determined in earlier single sensor DTA (SSDTA) nucleation study (Refs. 4 and 7);
- The single constant parameter for the interaction between the secondary and tertiary γ' particles (Eq. (1)), as discussed earlier was determined;
- An adjustment for the tertiary γ' coarsening rate was found to be needed in order to avoid particle size over-estimation (by a factor of about 2, which is consistent with the slow isothermal coarsening kinetics for γ' particles discussed in the 2008 annual report (Ref. 7)).

Figure 4 shows the γ' microstructure evolution results from one of the calibration calculations (the last condition shown in Table 2). During isothermal aging steps, secondary γ' size and fraction (green) increased, while tertiary fraction decreased, demonstrating the secondary/tertiary interaction. Without this regulated interaction, the mean field assumption would cause a complete dissolution of tertiary γ' too quickly. Note that there was an increase of tertiary γ' size during cooling right after the 855 °C aging.

Next we applied the calibrated parameters to the entire available dataset of supersolvus LSHR discussed in Reference 6. Both experimental data and predictions are summarized in Table 3 and graphically in Figure 5. In Table 3, both experimental median and mean (3–D) particle sizes are listed. For multistep *PrecipiCalc* predictions, 3–D mean sizes are reported. For tertiary γ' particles, the sizes at the end of the last aging step (before subsequent final cooling) and at the end of the simulation (after final cooling) are reported. It was observed the final cooling could increase the tertiary size by growth, or decrease it by

nucleation (generation of smaller γ' particle into the same tertiary distribution). In both cases, the volume fraction of tertiary γ' precipitates increased during the final cooling step. This could represent the potential microstructure variation due to the approximation of cooling rate during the final cooling. The green and red colors are used for slow and fast quenching from supersolvus solution treatment, respectively, in both Table 3 and Figure 5. The symbols in the last column of Table 3 represent the plot symbols used in Figure 5. That is, triangles for as solution treated condition, diamonds for single step aging conditions, and squares for double step aging conditions.

TABLE 3.—CALIBRATION AND VALIDATION RESULTS OF γ' MICROSTRUCTURE FOR SUPERSOLVUS TREATED LSHR

			Experiments						Prediction				
			Secondary			Tertiary			Secondary		Tertiary		
Solution treat	Age 1	Age 2	Median radius (nm)	Mean radius (nm)	Volume fraction (%)	Median radius (nm)	Mean radius (nm)	Volume fraction (%)	Radius (nm)	Fraction (%)	Radius (nm)	Volume fraction (%)	
1171 °C + 72 °C/m	0	0	135.1	132.1	50	4.4	6.3	8	134.7	44.5	7.0	7.4	Δ
1171 °C + 72 °C/m	775 °C/8 hr	0	115.4	111.0	52	6.1	6.5	6	135.1	44.9	7.3/7.7	7.3/8.1	◊
1171 °C + 72 °C/m	815 °C/8 hr	0	115.1	111.6	57	9.9	10.3	1	136.0	45.7	8.0/8.9	5.5/7.0	◊
1171 °C + 72 °C/m	855 °C/1 hr	0	134.0	133.6	53	10.8	10.9	5	135.2	44.9	8.1/9.9	4.9/7.8	◊
1171 °C + 72 °C/m	855 °C/8 hr	0	116.0	112.1	57	14.6	14.8	1	139.1	48.9	10.6/14.5	1.0/2.1	◊
1171 °C + 72 °C/m	855 °C/1 hr	775 °C/8 hr	119.7	118.2	54	9.1	9.3	4	135.3	45.0	9.8/10.5	7.2/7.5	□
1171 °C + 72 °C/m	855 °C/4 hr	775 °C/8 hr	155.0	142.0	51	13.2	14.0	7	136.9	46.6	11.7/12.3	5.6/5.6	□
1171 °C + 72 °C/m	855 °C/8 hr	775 °C/8 hr	139.2	140.0	57	15.3	14.5	1	142.2	52.3	15.4/0.8	0/2	□
1171 °C + 202 °C/m	0	0	75.6	75.2	54	2.7	3.5	4	75.2	45.0	4.0	6.4	Δ
1171 °C + 202 °C/m	775 °C/8 hr	0	61.2	61.0	55	5.1	5.2	3	75.3	45.2	5.0/5.3	7.0/8.1	◊
1171 °C + 202 °C/m	815 °C/3 hr	0	77.5	77.3	57	6.8	7.4	1	75.4	45.2	5.8/6.6	5.9/7.8	◊
1171 °C + 202 °C/m	815 °C/8 hr	0	89.4	89.1	57	9.4	9.6	1	75.7	45.9	7.1/8.0	5.3/6.9	◊
1171 °C + 202 °C/m	855 °C/1 hr	0	70.3	71.4	54	8.1	8.1	4	75.3	45.2	7.2/9.2	4.6/7.6	◊
1171 °C + 202 °C/m	855 °C/8 hr	0	70.4	70.9	58	15.0	14.2	0.1	77.4	49.0	12.1/16.0	0.9/1.9	◊
1171 °C + 202 °C/m	855 °C/1 hr	775 °C/8 hr	96.7	97.1	56	10.5	11.0	2	75.4	45.3	9.1/9.8	6.9/7.3	□
1171 °C + 202 °C/m	855 °C/4 hr	775 °C/8 hr	62.9	62.4	55	11.0	11.3	3	76.1	46.5	11.8/12.3	5.7/5.8	□
1171 °C + 202 °C/m	855 °C/8 hr	775 °C/8 hr	78.5	78.9	56	14.5	15.4	0.1	79.1	52.3	16.9/4.7	0/0	□

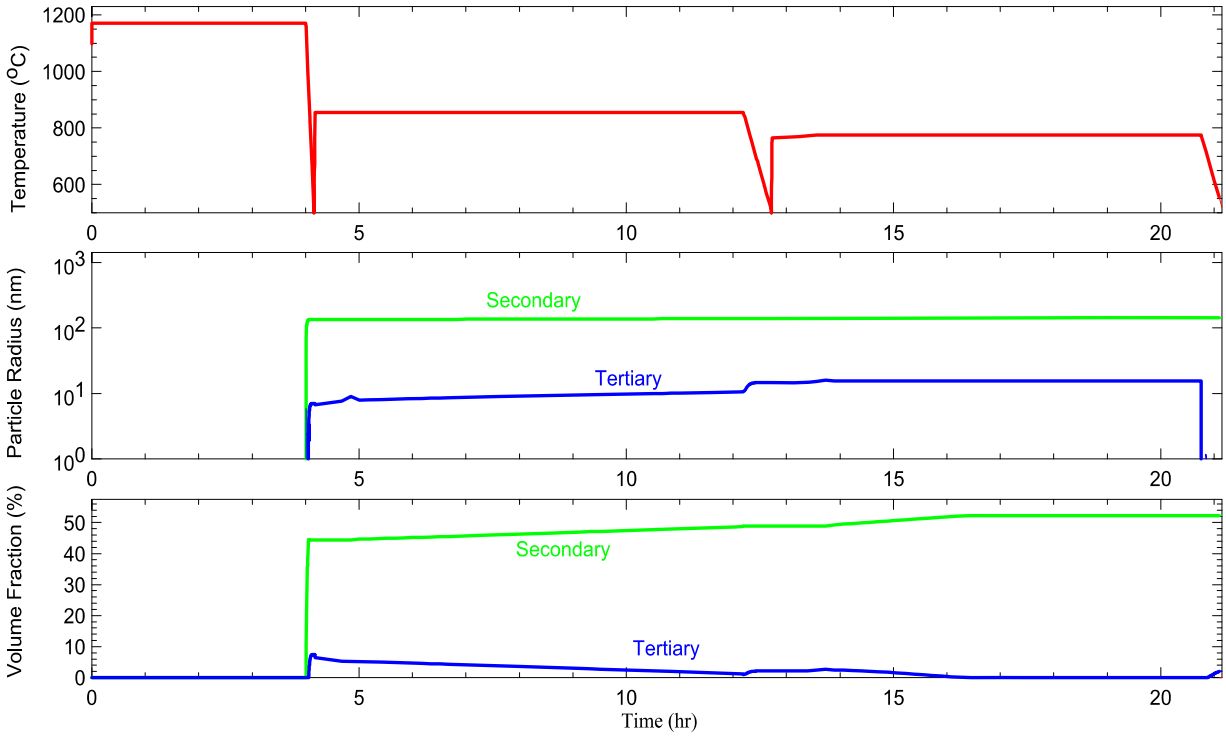

Figure 4.—An example calculation results are shown below for the case with a treatment condition: 1171 °C/4 hr + 72 °C/m + 855 °C/8 hr + 775 °C/8 hr.

In the plot of secondary particle size in Figure 5(a), experimental measurements are shown to have a larger variation than the model prediction. However, there was no correlation in experimental values with respect to the heat treatment parameters (Ref. 6). Hence, the prediction of secondary γ' sizes were considered accurate. There was a consistent discrepancy that experimental secondary γ' fractions are higher than the prediction, as shown in Figure 5(b). Several possibilities have been discussed, including experimental artifacts (etching and 3–D effects) and thermodynamics database inaccuracy, but no definite reasons have been concluded. This deserves further investigation to determine the cause of discrepancy.

For the tertiary γ' microstructure in Figure 5, only the prediction at the end of last aging (before final cooling) was used. The tertiary γ' size, Figure 5(c), showed a good correlation between experiments and prediction. The multistep *PrecipiCalc* framework predicted the correct trend and reasonable values of tertiary radii with respect to the heat treatment condition. The predicted volume fraction of tertiary γ' had a scattered correlation with the experimental data, but was well within the correct range of phase fraction. With the higher potential variability in experimental volume fraction measurement, the prediction was considered satisfactory.

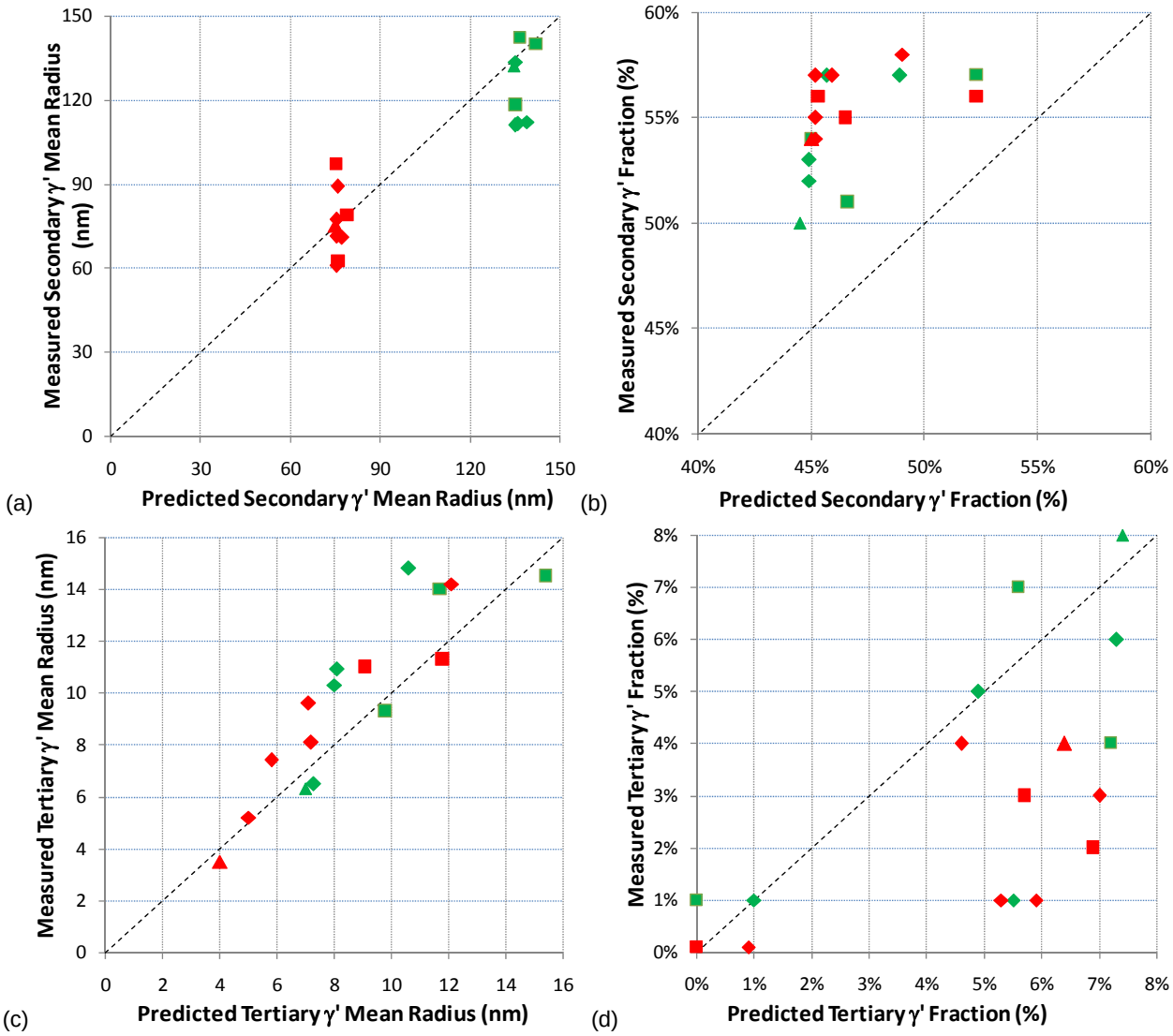

Figure 5.—Correlation plot of γ' microstructure for supersolvus treated LSHR samples. (a),(b) for secondary and (c),(d) for tertiary γ'. (a),(c) for mean radii and (b),(d) for volume fraction. The diagonal dash lines represent perfect correlation.

γ' Microstructure Modeling and Misfit Prediction with JMATPro

An LSHR sample was sent to University of Cambridge for analyses by synchrotron/neutron diffraction to measure γ/γ' room temperature misfit, and a value of +0.026 percent was estimated. This subsection summarizes an attempt to predict misfit by combining *PrecipiCalc* and JMATPro (Sente Scientific) software tools.

Based on a simulated temperature profile provided by NASA (see Figure 6) at the location where the LSHR misfit sample was taken, a *PrecipiCalc* quenching simulation was conducted. Final secondary γ' was predicted to be 47 percent, in good agreement with the 45 percent estimated by neutron diffraction. Based on the *PrecipiCalc* simulation results, two temperatures (1094 and 956 °C, representing 50 and 90 percent secondary γ' completion) were used by GRC for predicting the associated γ and γ' compositions, and room temperature misfit, using JMATPro-Ni 5.0 software (Ref. 2), to compare with the misfit measurement.

The JMATPro results shown in Figure 7 indicate that the room temperature misfit prediction using the compositions at 50 and 90 percent completion does bracket the experimental measurement (thick arrows). JMATPro results also indicate fairly strong composition dependency in misfit. This brings up a consideration of significance for location-specific misfit driven by varying γ' microstructure and compositions.

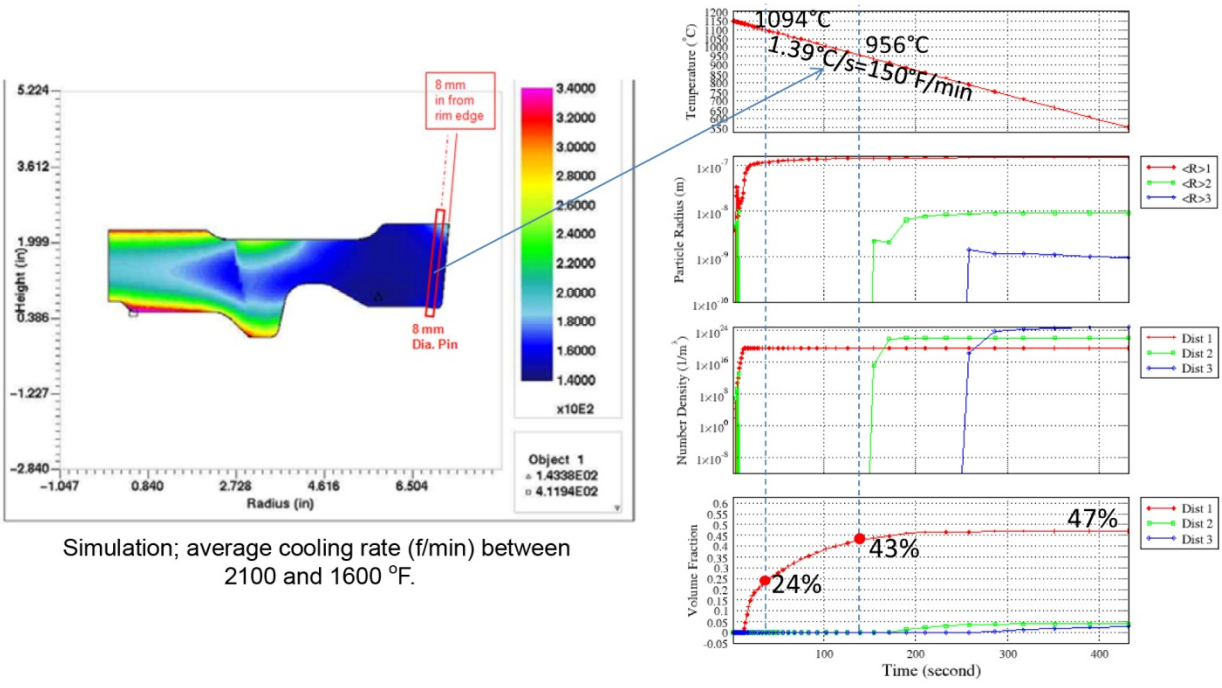

Figure 6.—*PrecipiCalc* simulation for LSHR sample used in misfit measurement.

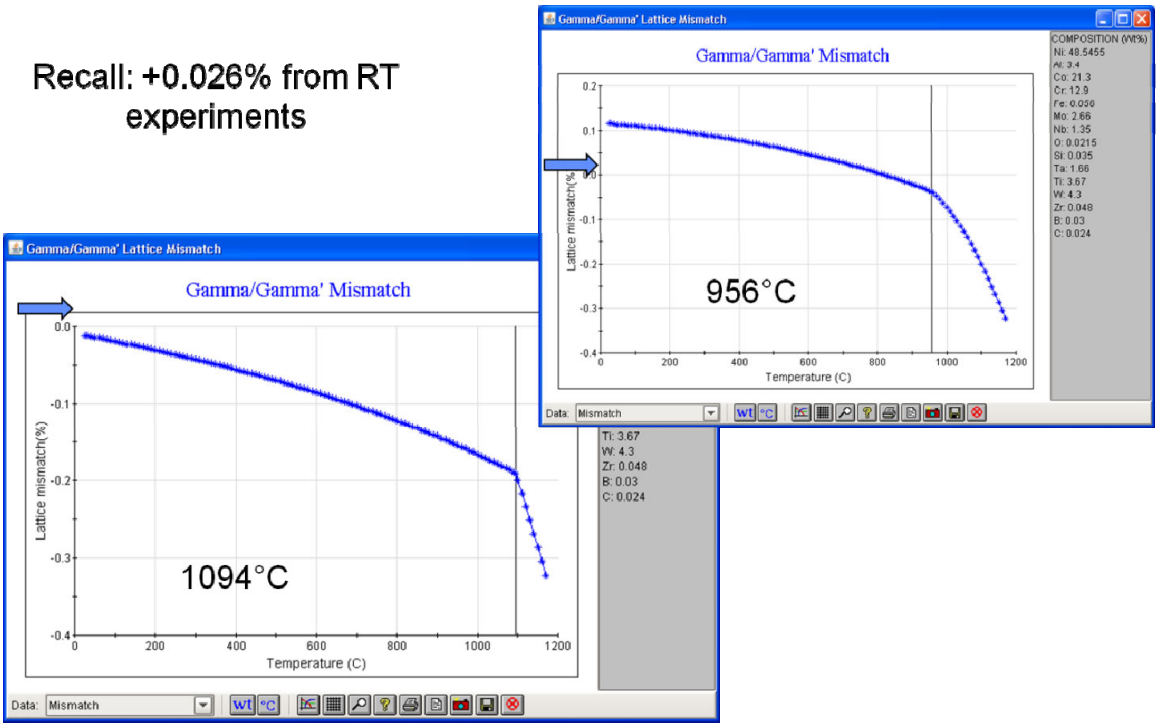

Figure 7.—JMATPro misfit prediction for an LSHR sample and comparison with experimental measurement indicated by the large blue arrows.

Task 4—Precipitation Modeling of Minor Phases

Several minor precipitate phases in Ni-based aeroturbine disk alloys, including carbides, borides and intermetallics, can nucleate or evolve during the long term thermal exposure during service. These minor phases can affect the performance of the disk component, and thus is desirable to model the precipitation evolution of the aforementioned phases during thermal exposure.

Summary of Experimental Results

GRC conducted experimental characterization of minor phases in LSHR—carbides (including MC and $M_{23}C_6$), boride (M_3B_2) and topological close packed TCP (σ) phases. LSHR samples having different process histories were investigated, including extrusion, forging, supersolvus solution treatment at 1199 °C (followed by water quench or furnace quench), and one single aging step at three isothermal aging temperatures (760, 843 and 927 °C) for three different hold times (10, 100 and 1000 hr), spanning heat treatment to prolonged service conditions. SEM/EDS and TEM were used at GRC to identify the phase and microstructure of the precipitates. The detailed experiment and analysis procedures will be published by GRC researchers. Table 4 summarizes the mean radii and volume fraction of the minor phases in characterized LSHR samples. Figure 8 presents the data with the thermal history on the x-axis.

TABLE 4.—A SUMMARY OF GRC EXPERIMENTAL MINOR PHASE CHARACTERIZATION ON LSHR HEAT TREATED UNDER DIFFERENT CONDITIONS

		MC		$M_{23}C_6$		M_3B_2		σ	
ID	Conditions	<R>, μm	vf, %	<R>, μm	vf, %	<R>, μm	vf, %	<R>, μm	vf, %
1	As Extruded	0.137	0.08	0	0	0.256	0.351	0	0
2	1 + Forging	0.155	0.1	0	0	0.299	0.121	0	0
3	2 + 1199 °C/1 hr + F. Cool	0.186	0.196	0	0	0	0	0	0
4	2 + 1199 °C/1 hr + WQ	0.173	0.161	0	0	0.178	0.002	0	0
5	4 + 760 °C/10 hr+ WQ	0.163	0.161	0	0	0	0	0	0
6	4 + 760 °C/100 hr + WQ	0.173	0.189	0.104	0.015	0.364	0.033	0	0
7	4 + 760 °C/1000 hr + WQ	0.179	0.217	0.171	0.148	0.18	0.054	0	0
8	4 + 843 °C/10 hr + WQ	0.194	0.259	0.077	0.003	0.077	0.001	0	0
9	4 + 843 °C/100 hr + WQ	0.198	0.219	0.144	0.095	0	0	0.196	0.058
10	4 + 843 °C/1000 hr + WQ	0.195	0.184	0.288	0.418	0.383	0.042	0.265	0.327
11	4 + 927 °C/10 hr + WQ	0.196	0.162	0.147	0.136	0.46	0.0005	0.174	0.053
12	4 + 927 °C/99 hr + WQ	0.187	0.126	0	0	0.6	0.0005	0.191	0.024
13	4 + 927 °C/1000 hr + WQ	0.198	0.3	0	0	1.139	0.827	0	0

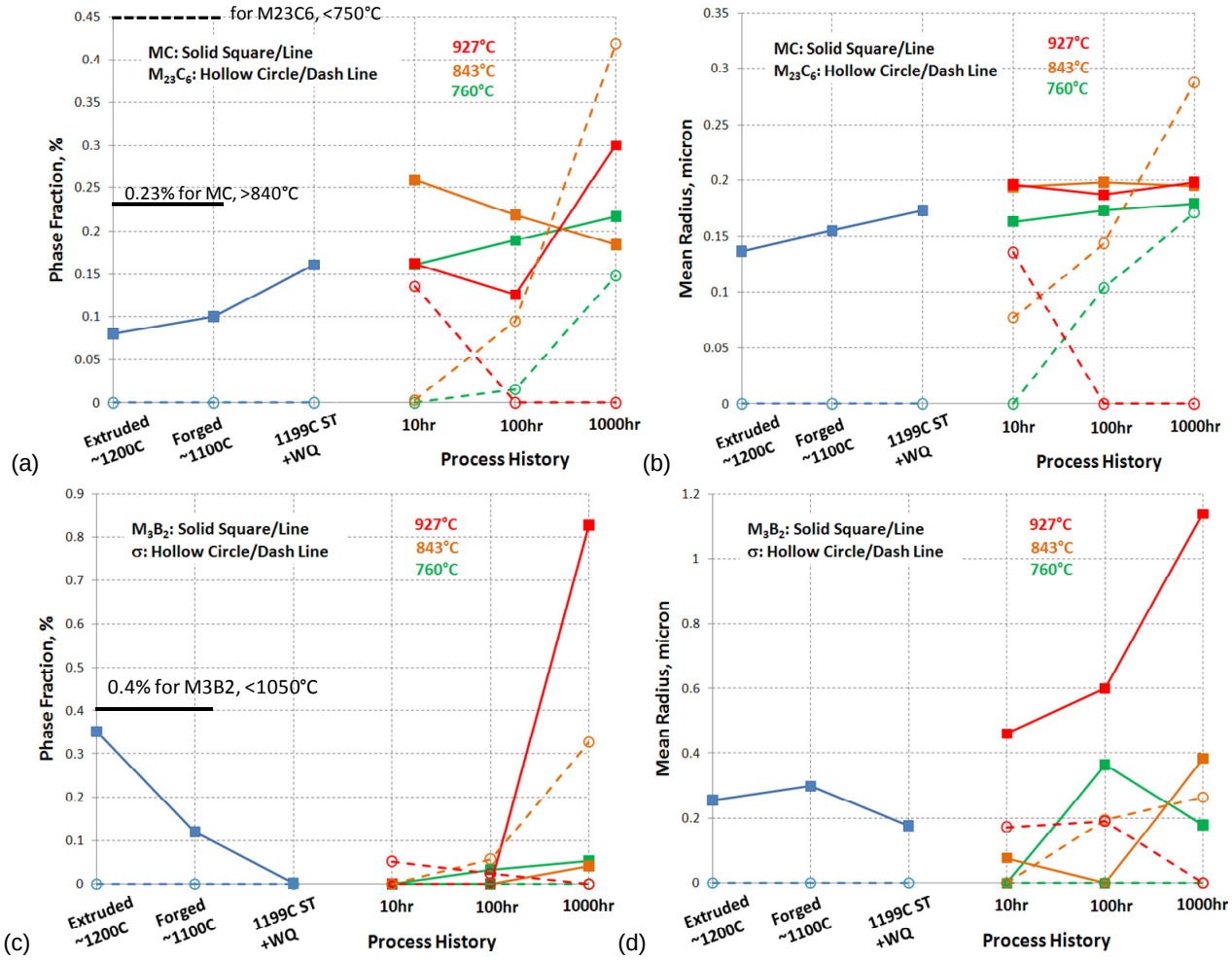

Figure 8.—Graphical representation of the minor phase microstructure data in Table 4. Carbides microstructure is shown in (a) and (b), while microstructure of boride and σ phases are shown in (c) and (d). The black horizontal lines in (a),(c) represent the equilibrium phase fraction predicted by *PrecipCalc* using the Ni-Data v7 database.

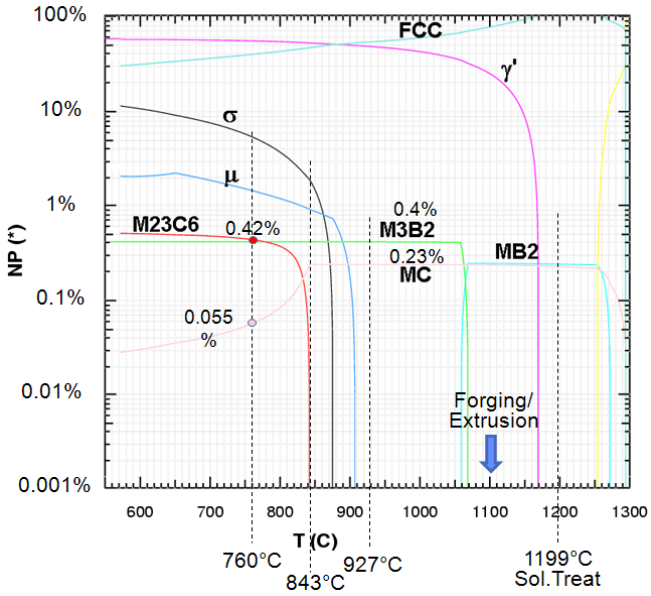

Figure 9.—Phase fractions in LSHR (denoted as NP) at equilibrium as functions of temperature, predicted by *ThermoCalc* using the Ni-Data version 7 database.

Thermodynamics Investigation

Equilibrium predictions of phase fractions versus temperature are shown in Figure 9. It is worth noting that, M_3B_2 is not stable during extrusion/forging/solution treatment, and replacement of MC with $M_{23}C_6$ was predicted below 841 °C. When all TCP phases are suspended in the calculation, $M_{23}C_6$ solvus temperature increased by 10 °C. The σ and μ phases appeared to have high equilibrium fraction, but are usually limited by slow formation kinetics. When both σ and μ are suspended in the calculation, P phase appeared in a similar temperature range with a similar phase fraction as that of μ phase.

Within 700 to 900 °C where isothermal aging was conducted for LSHR samples, the predicted phase compositions (in atomic fraction) are:

σ	$Cr_{0.50}Co_{0.30}Ni_{0.10}Mo_{0.07}W_{0.01}$
μ	$Co_{0.30}Mo_{0.22}Cr_{0.17}Ni_{0.15}W_{0.14}$
P-phase	$Cr_{0.28}Co_{0.20}W_{0.18}Mo_{0.17}Ni_{0.16}$
M_3B_2	$Mo_{0.38}$-$Cr_{0.21}$-$W_{0.01}$-$B_{0.40}$
$M_{23}C_6$	$Cr_{0.60}$-$Mo_{0.09}$-$Co_{0.05}$-$W_{0.01}$-$C_{0.21}$
MC	$Ti_{0.12}$-$Nb_{0.16}$-$Ta_{0.15}$-$Zr_{0.08}$-$C_{0.49}$

The major components in the individual phases were mostly in agreement with GRC's experimental observation. One major exception is M_3B_2, where there was experimental evidence of high W content. In addition, GRC's experiments found that, in some aging conditions, a very small amount of a Mo,Ti, and Cr-rich phase appeared with cylindrical morphology. However, there were no Mo, Ti, and Cr rich phases predicted. More quantitative experimental composition measurements would be beneficial to confirm the current measurements and to clarify the composition discrepancy between experiments and predictions.

Comparing Figure 9 and Figure 8, several inferences can be made:

- Prior to aging, MC phase fraction was increasing towards the equilibrium predicted phase fraction. There was no $M_{23}C_6$ found in the as-quench condition prior to aging treatments.

- At 927 °C, MC fraction increased while amount of $M_{23}C_6$ decreased, which was compatible with thermodynamics predictions. However, the observed $M_{23}C_6$ at 10 hr aging might be formed during heat up to 927 °C.
- At 843 °C, replacement of MC by $M_{23}C_6$ occurred. This indicates that $M_{23}C_6$ had higher thermal stability than predicted by the thermodynamics. However, MC fraction at 10 hr was higher than the equilibrium value, which was unexpected.
- At 760 °C, fraction of both carbides increased but were still below their equilibrium values at 1000 hr. According to thermodynamics, the amount of MC carbides will eventually decrease to feed additional $M_{23}C_6$ formation.
- Overall effect of aging time on MC size was smaller than that on $M_{23}C_6$ size. Several higher than equilibrium fractions were observed experimentally. The simulations, however, are not expected to capture those high volume fractions.
- M_3B_2 dissolves prior to aging, which was compatible with equilibrium prediction. During the dissolution of M_3B_2, there was no experimental observation of MB_2 phase. It is desirable to determine whether boron stays in solution, or less probably in few large MB_2 particles which are difficult to find.
- M_3B_2 amount increased during aging, with a fast transformation kinetics at 927 °C. M_3B_2 amount was in general far from equilibrium, except at 927 °C/1000 hr.
- σ phase amount increased at 843 °C, while dissolving at 927 °C, again compatible with equilibrium prediction. But overall, σ phase amount was far from equilibrium, and precipitation kinetics of σ phase was extremely slow at 760 °C.

The three plots in Figure 10 summarize the precipitation trajectory of MC and $M_{23}C_6$ carbides based on an unstable equilibrium fraction-supersaturation relationship. This information helped us understand the precipitation path along the thermodynamic supersaturation, and provided calibration input for multiphase simulation.

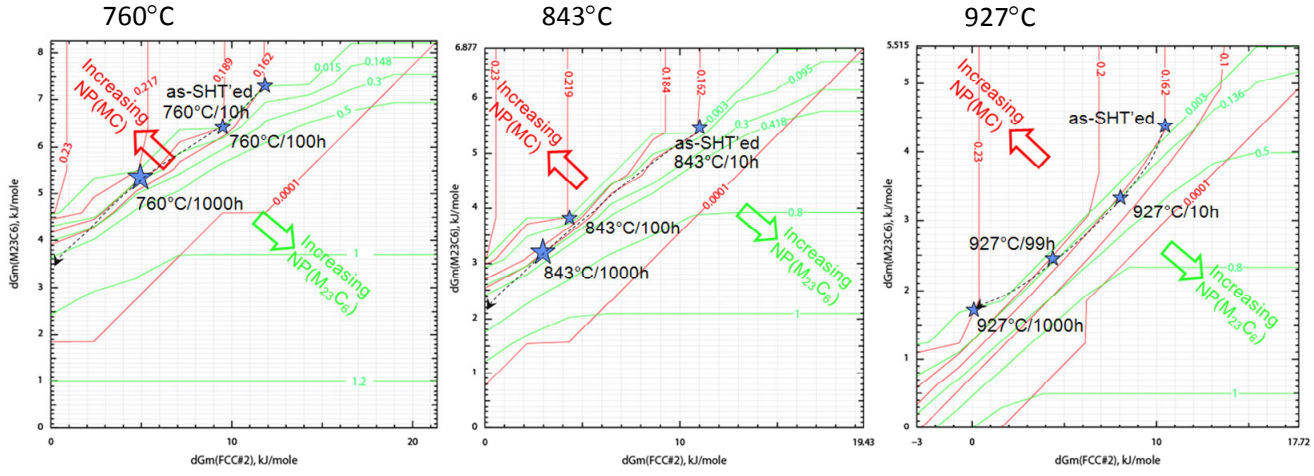

Figure 10.—Trajectory evaluation of carbides at the three isothermal aging temperatures. Driving force of MC ($M_{23}C_6$) is shown in the X- (Y-) axis. The stars represent the experimentally observed carbide fractions. The precipitation trajectory is formed by connecting the stars.

Multiphase PrecipiCalc Simulations of Carbides

This subsection summarizes the application of *PrecipiCalc* software to simulate the concurrent MC and $M_{23}C_6$ carbide microstructure evolution during isothermal aging. As discussed in the equilibrium study above, several unexpected phase fractions were observed, and *PrecipiCalc* simulations were not expected to capture those observations quantitatively. Hence, our key simulation objective was to capture the qualitative trend while attempting to capture the quantitative values as much as possible. In order to achieve a manageable simulation complexity, the simulations focused on the carbides by assuming that:

- γ' reaches equilibrium a lot faster than carbides (for example, γ' volume fraction is fairly constant after 1 hr aging at 775 °C γ' by simulation)—this allowed us to remove the γ' phase at ~53 percent phase amount, and focus on the remaining 47 percent of the carbides precipitation in FCC simulation.
- Slow kinetics for borides and TCP—this allowed us to ignore these phases.

The starting microstructure at the beginning of the simulation had no $M_{23}C_6$, and the amount of MC was assumed to be 0.161 percent at a mean size of 0.163 μm, corresponding to the as-quenched microstructure. A normal distribution with a standard deviation of 0.02 μm was used to describe the initial MC particle size distribution. In addition, a homogeneous nucleation (intragrain) model was used for MC, while grain boundary heterogeneous nucleation model was used for $M_{23}C_6$. By investigating the $M_{23}C_6$ morphology observed by NASA, see Figure 11 as an example, a grain size of 32 μm and a wetting angle of 32° were used. The LSHR overall composition used was Ni-3.4Al-12.9Cr-21.3Co-3.67Ti-2.66Mo-4.3W-1.35Nb-1.66Ta-0.048Zr-0.024C-0.03B (in wt%).

By calibrating to experimental data, key precipitation parameters were determined:

- MC/FCC surface energy: 0.8 J/m^2 for all three temperatures
- $M_{23}C_6$/FCC surface energy: a linear dependency with temperature, see Figure 12, provided the best overall fit to experimental data
- Diffusion scaling of 0.2 (to account for slower coarsening rate), and additional diffusion scaling of 0.005 for $M_{23}C_6$ due to its limited interaction with MC

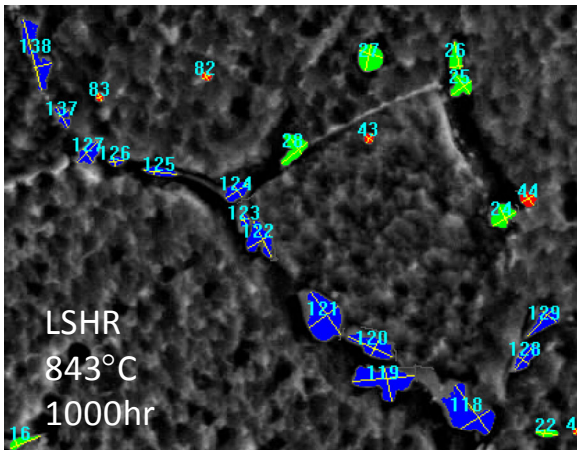

Figure 11.—A processed LSHR SEM micrograph showing blue $M_{23}C_6$ grain boundary carbides.

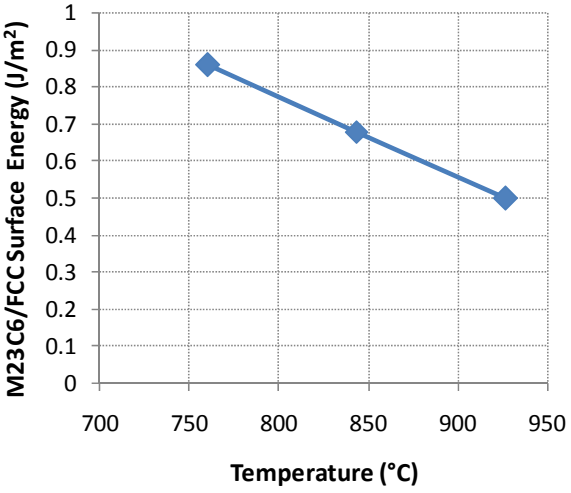

Figure 12.—$M_{23}C_6$ surface energy was taken to linearly depend on temperature consistent with positive surface entropy.

The results of the simulation are summarized in Figure 13. The overall microstructure evolution features were captured through simulation. However, several discrepancies, including small $M_{23}C_6$ size and faster MC dissolution near 1000 hr (driven by mass balance of carbon), demand further investigation in the future. The ignoring of γ', boride and TCP phases in these simulation could play some role in the discrepancies observed. In addition, the observed $M_{23}C_6$ at 927 °C/10 hr could be due to heating to aging temperature, which was not simulated as we only considered isothermal aging. Though they lack absolute accuracy for material engineering optimization, these simulation capabilities can already provide valuable insights into the carbide microstructure evolution.

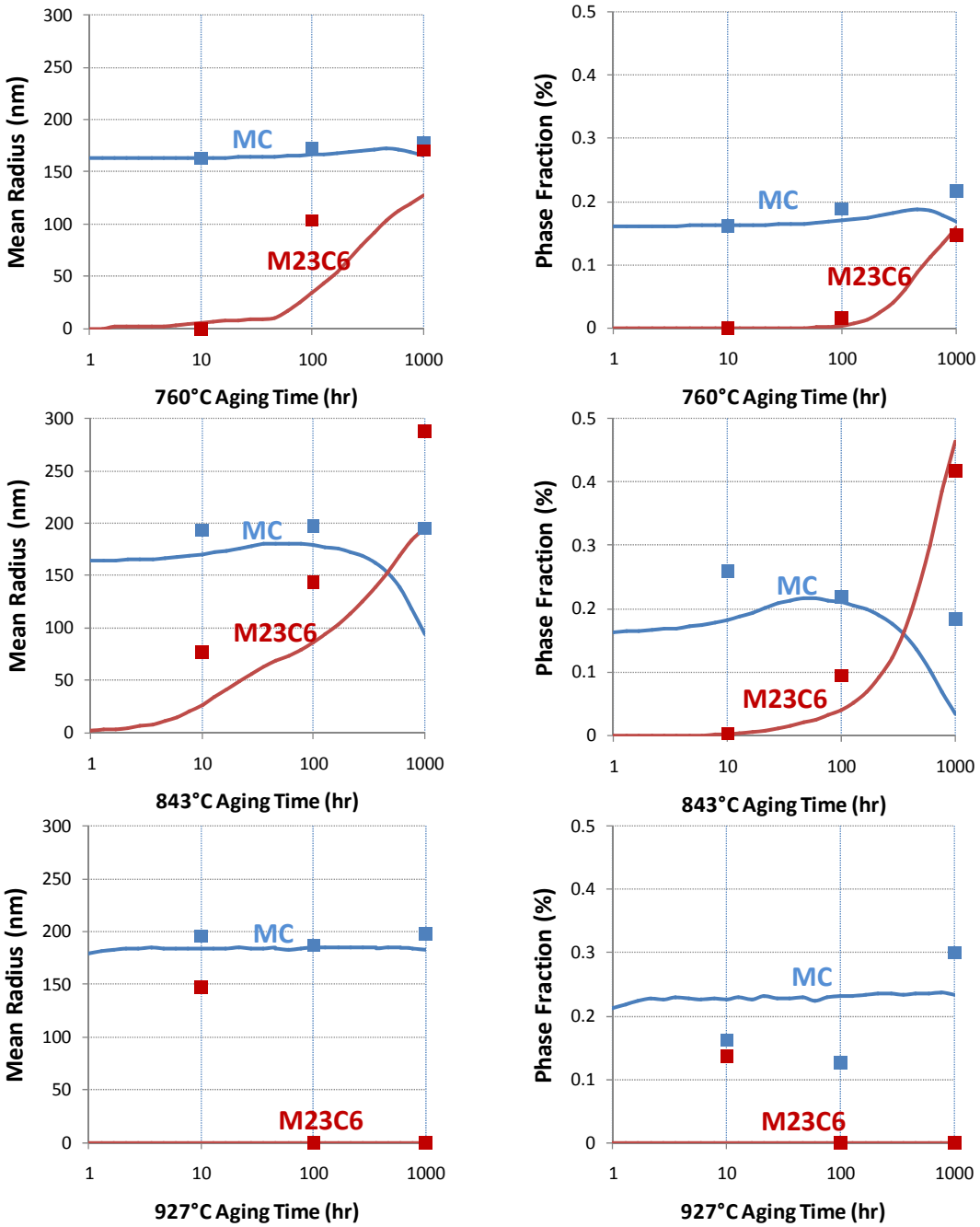

Figure 13.—Comparison of LSHR carbide microstructure evolution between experiments and predictions. NASA experimental results are in square points and *PrecipiCalc* simulation results are in solid curves. MC carbides are in blue and $M_{23}C_6$ carbide are in red.

Task 5—Software Implementation and Dissemination

Driven by the need to minimize the steep learning curve of *PrecipiCalc* software, this Task focused on producing user friendly precipitation simulation tools, based on *PrecipiCalc*, for aeroturbine disk material engineers. There were two software tools, one for γ' precipitation microstructure during heat treatment, and another for carbide precipitation microstructure during isothermal holding. Both set of software shared similar features: graphical user interface (GUI) for user friendly pre- and post-processing operation, cross platform implementation (using Java and Python) for easy transfer to other operating systems (tested on Microsoft Windows XP/7 and Linux), based on *PrecipiCalc* simulation software. Alpha and beta versions of the software were distributed during 2009, and the final version of the software was released at the end of 2009.

γ' Precipitation Simulation Tool

The detailed operating instruction of the software is described in a separate software manual. Here we summarize the key features of the software in relationship to the Task 3 modeling efforts described in the above Section. Figure 14 provides an overview of the software architecture, which includes three levels:

1. Graphical User Interface (GUI)—containing four separate modules of operation. Lookup table module allows user to input alloy composition and generate a lookup table file. Preprocessing module collects heat treatment conditions and material properties. Computing module starts and monitors calculation and post-processing module provides facility to view and plot results. GUI is written in Java (Sun Microsystems, Inc.) (http://www.java.com/) and PLPlot library (http://plplot.sourceforge.net/).
2. CALPHAD-based Programs—including *PrecipiCalc*, lookup table generation software, and a software for composition calculation with phases removal. These command line-based tools often use Thermo-Calc and were written in C/C++.
3. Wrapper Programs—these take the information provided by the GUI and operate the CALPHAD-based programs (no. 2 above) according to the developed algorithm, such as the multistep γ' simulation framework discussed in Task 3. The wrapper programs were command line-based and were written in Python (Python Software Foundation) (http://www.python.org/). In addition, wrapper programs can also be operated by a software robot (like iSIGHT) to enable large scale simulations.

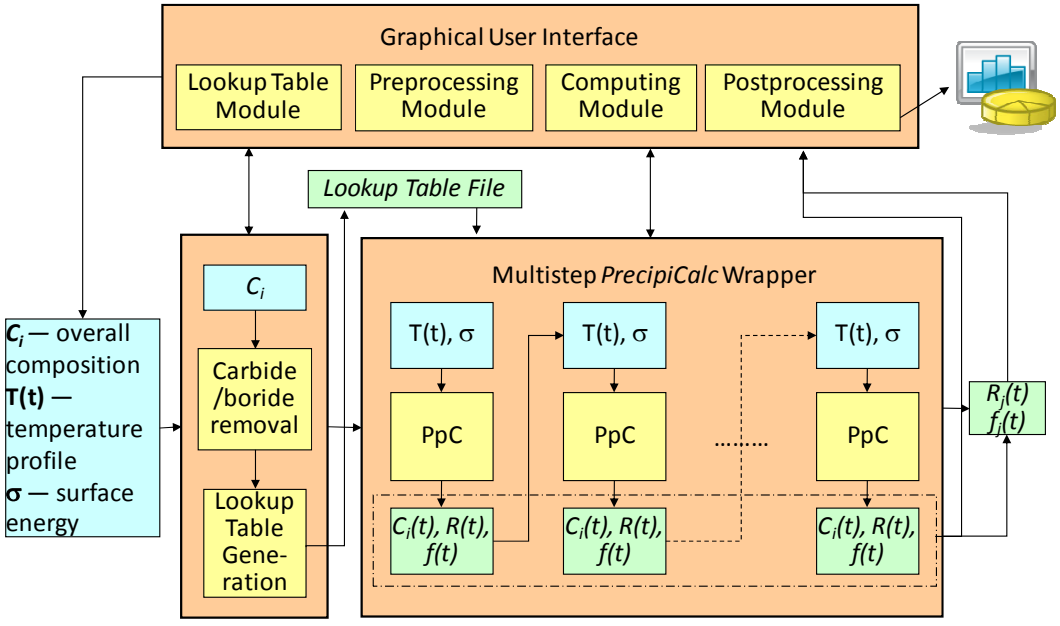

Figure 14.—Software implementation architecture for multistep *PrecipiCalc* (PpC) γ' microstructure simulations of heat treatment.

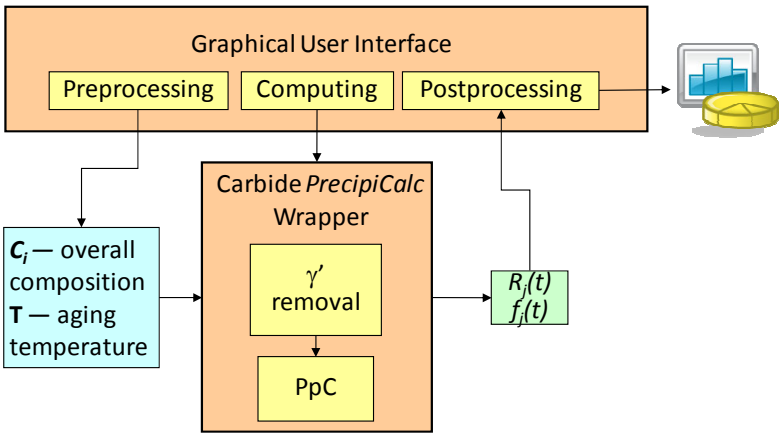

Figure 15.—Schematic diagram of the carbide precipitation simulation software.

Carbide Precipitation Simulation Tool

Like the γ' simulation tool, the carbide precipitation simulation tool, capturing the carbide simulations discussed in Task 4 of this report, also contains three levels of software—GUI, CALPHAD-based tools and wrapper programs. It has simpler GUI module and wrapper components than those in the γ' simulation program.

Conclusions

At the conclusion of this third year NASA program, extensive development of precipitation microstructure evolution was made for Ni-based disk superalloys in the following areas:

- **γ' Precipitation Modeling**
  - Successful development of multistep *PrecipiCalc* framework to eliminate mean field limitation
  - Reasonable calibration and validation of multistep *PrecipiCalc* framework against supersolvus treated LSHR with systematic discrepancy in phase fraction comparison
  - Implementation of the framework into a user friendly software tool
  - Slow γ' coarsening rate calibrated, but deserves further study by the Ni-based superalloys research community in order to determine a physics-based mechanism

- **Carbide Precipitation Modeling**
  - Equilibrium study identified mismatches between experimental results and thermodynamics database
  - Successful demonstration of multiphase *PrecipiCalc* simulation for concurrent MC and $M_{23}C_6$ carbide microstructure evolution during long term aging
  - Qualitative carbide microstructure features with complex interaction were predicted
  - Implementation of software into a user friendly software tool

- **Software Dissemination**—the software components developed under this program was delivered to NASA and project collaborators at the end of this program.

Though model calibration/validation was mainly established with data of NASA's LSHR alloy in this report, the tool can be used to support modeling efforts for other alloys, such as Rolls-Royce's RR1000 alloy.

References

1. A.M. Wusatowska-Sarnek, G. Ghosh, G.B. Olson, M.J. Blackburn, and M. Aindow, *J. Materials Research*, 18 (2003) 2653–2663.
2. N. Saunders, Z. Guo, X. Li, A.P. Miodownik, J-Ph. Schille, *Superalloys 2004*, eds. K.A. Green, T.M. Pollock, H. Harada, T.E. Howson, R.C. Reed, J.J. Schirra, and S. Walston, (2004) 849–858. http://www.sentesoftware.co.uk/jmatpro-version-50-released.aspx
3. H.-J. Jou, Microstructure Modeling of 3rd Generation Disk Alloys—1st Annual Report, December 2007, http://ntrs.nasa.gov/archive/nasa/casi.ntrs.nasa.gov/20080021187_2008019927.pdf
4. H.-J. Jou, Microstructure Modeling of 3rd Generation Disk Alloys—2nd Annual Report, December 2008.
5. H.-J. Jou, P. Voorhees and G.B. Olson, *Superalloys 2004*, eds. K.A. Green, T.M. Pollock, H. Harada, T.E. Howson, R.C. Reed, J.J. Schirra, and S. Walston, (2004) 877–886.
6. T. Gabb, J. Gayda, J. Telesman, A. Garg, *Superalloys 2008*, eds. R.C. Reed, K.A. Green, P. Caron, T.P. Gabb, M.G. Fahrmann, E.S. Huron, and S.A. Woodward, TMS (The Minerals, Metals, & Materials Society), (2008) 121.
7. G.B. Olson, H.-J. Jou, J. Jung, J.T. Sebastian, A. Misra, I. Locci and D. Hull, *Superalloys 2008*, eds. R.C. Reed, K.A. Green, P. Caron, T.P. Gabb, M.G. Fahrmann, E.S. Huron, and S.A. Woodward, TMS (The Minerals, Metals, & Materials Society), (2008) 923–932. http://ntrs.nasa.gov/archive/nasa/casi.ntrs.nasa.gov/20090004682_2009001242.pdf

REPORT DOCUMENTATION PAGE		Form Approved OMB No. 0704-0188

1. REPORT DATE (DD-MM-YYYY)	2. REPORT TYPE	3. DATES COVERED (From - To)
01-07-2010	Final Contractor Report	December 16, 2008 - December 31, 2009

4. TITLE AND SUBTITLE
Microstructure Modeling of Third Generation Disk Alloys
Final Report

5a. CONTRACT NUMBER
NNC07CB01C

5b. GRANT NUMBER

5c. PROGRAM ELEMENT NUMBER

6. AUTHOR(S)
Jou, Herng-Jeng

5d. PROJECT NUMBER

5e. TASK NUMBER

5f. WORK UNIT NUMBER
WBS 698259.02.07.03.04.02

7. PERFORMING ORGANIZATION NAME(S) AND ADDRESS(ES)
QuesTek Innovations LLC
1820 Ridge Avenue
Evanston, Illinois 60201

8. PERFORMING ORGANIZATION REPORT NUMBER
E-17325

9. SPONSORING/MONITORING AGENCY NAME(S) AND ADDRESS(ES)
National Aeronautics and Space Administration
Washington, DC 20546-0001

10. SPONSORING/MONITOR'S ACRONYM(S)
NASA

11. SPONSORING/MONITORING REPORT NUMBER
NASA/CR-2010-216748

12. DISTRIBUTION/AVAILABILITY STATEMENT
Unclassified-Unlimited
Subject Category: 07
Available electronically at http://gltrs.grc.nasa.gov
This publication is available from the NASA Center for AeroSpace Information, 443-757-5802

13. SUPPLEMENTARY NOTES

14. ABSTRACT
The objective of this program was to model, validate, and predict the precipitation microstructure evolution, using PrecipiCalc (QuesTek Innovations LLC) software, for 3rd generation Ni-based gas turbine disc superalloys during processing and service, with a set of logical and consistent experiments and characterizations. Furthermore, within this program, the originally research-oriented microstructure simulation tool was to be further improved and implemented to be a useful and user-friendly engineering tool. In this report, the key accomplishments achieved during the third year (2009) of the program are summarized. The activities of this year included: Further development of multistep precipitation simulation framework for γ' microstructure evolution during heat treatment; Calibration and validation of γ' microstructure modeling with supersolvus heat treated LSHR; Modeling of the microstructure evolution of the minor phases, particularly carbides, during isothermal aging, representing the long term microstructure stability during thermal exposure; and the implementation of software tools. During the research and development efforts to extend the precipitation microstructure modeling and prediction capability in this 3-year program, we identified a hurdle, related to slow γ′ coarsening rate, with no satisfactory scientific explanation currently available. It is desirable to raise this issue to the Ni-based superalloys research community, with hope that in future there will be a mechanistic understanding and physics-based treatment to overcome the hurdle. In the mean time, an empirical correction factor was developed in this modeling effort to capture the experimental observations.

15. SUBJECT TERMS
Gas turbine engines; Rotating disks; Heat resistant alloys

16. SECURITY CLASSIFICATION OF:			17. LIMITATION OF ABSTRACT	18. NUMBER OF PAGES	19a. NAME OF RESPONSIBLE PERSON
a. REPORT	b. ABSTRACT	c. THIS PAGE			STI Help Desk (email:help@sti.nasa.gov)
U	U	U	UU	25	19b. TELEPHONE NUMBER (include area code) 443-757-5802